[2] K. Kant and S. W. Zucker, "Toward efficient trajectory planning: The path-velocity decomposition," *Int. J. Robotics Res.*, vol. 5, no. 3, pp. 72–89, Fall, 1986.
[3] B. H. Lee and C. S. G. Lee, "Collision-free motion planning of two robots," *IEEE Trans. Syst. Man Cybern.*, vol. SMC-17, no. 1, pp. 21–32, 1987.
[4] J. E. Bobrow, S. Dubowsky, and P. Gibson, "On the optimal control of robotic manipulators with actuator constraints," in *Proc. Automat. Contr. Conf.*, June 1983, pp. 782–787.
[5] K. G. Shin and N. D. McKay, "Minimum–time control of robotic manipulators with geometric path constraints," *IEEE Trans. Automat. Contr.*, vol. AC–30, no. 6, pp. 531–541, June 1985.
[6] ——, "Robust trajectory planning for robotic manipulators under payload uncertainties," *IEEE Trans. Automat. Contr.*, vol. AC-32, no. 12, pp. 1044–1054, Dec. 1987.
[7] K. G. Shin and Q. Zheng, "Minimum time trajectory planning for dual robot systems," in *Proc. Contr. Decision Conf.*, Dec. 1989, pp. 2506–2511.
[8] E. Freund and H. Hoyer, "Pathfinding in multi-robot systems: Solution and applications," in *Proc. IEEE Int. Conf. Robotics Automat.*, vol. 1, 1986, pp. 103–111.

Multiple-Goal Kinematic Optimization of a Parallel Spherical Mechanism with Actuator Redundancy

Ronald Kurtz and Vincent Hayward

Abstract—**A new kinematic design will be presented that is fully parallel and actuator redundant. Actuator redundancy refers to the use of more actuators than are strictly necessary to control the mechanism without increasing the mobility. The uses of this form of redundancy include the ability to partially control the internal forces, increase the workspace, remove singularities, and augment the dexterity. Optimization will take place based on several objective functions. The kinematic dexterity, the forces present at the actuators, and the uniformity of the dexterity over the workspace will all be investigated as potential objectives. Global measures will be derived from each of these quantities for optimization purposes. Examining only a single objective may not yield an acceptable design. Instead, optimization of several factors is done simultaneously by specifying a primary objective and minimum performance standards for the secondary measures.**

I. Introduction

Parallel kinematic structures are important means to improve the performance of robot manipulators. Justifications for this have been extensively discussed in the literature, for example [10], [13], [15], in terms of structural and actuator advantages. Much attention have been devoted to the analysis of these structures from the kinematic (position and velocity) and dynamic viewpoints. A survey of these techniques, even partial, would be quite impossible to fit here, so references will be made as needed.

Of the immense number of possibilities offered by parallel kinematic structures, it appears that two have been extensively used: the pantograph mechanism and its derivatives (vast numbers of industrial manipulators), and the iso-static (or Stewart) platform. Many others have been proposed and used, but once again, a survey would be outside the scope of this paper.

The observation of biological manipulators was used to suggest alternate structures that could contribute to the design of manipulators. From a kinematic viewpoint, dualities between serial and parallel mechanisms have been pointed out [17]. One of them is not often discussed: the relative work volume for a given mechanical mobility. Serial chains have a large workspace (and poor structural properties); parallel ones have a reduced workspace (but good structural properties). It is not surprising that biological manipulators have hybrid structures: bones, tendons, and skeletal muscles form numerous chains closed regionally, yet the general architecture of biological manipulators is serial [8]. In addition, the work volume of biological manipulators can be large, for example, the human arm [12].

Part of the human shoulder can be approximated by a spherical ball and socket joint actuated by six muscle groups to control three degrees of freedom when four are strictly needed. This can be viewed as a case of actuator redundancy in which the redundant shoulder muscles are used to supply the internal forces needed to keep the humeral head (ball) firmly anchored to the glenoid (socket) throughout a large workspace. It also can be viewed as a means to increase workspace, among many other plausible interpretations such as the possibilities offered by antagonist actuation. This has inspired the development of a mechanical counterpart with similar properties: a three-degree-of-freedom mechanism fully parallel and actuator redundant. A detailed kinematic analysis has revealed that actuator redundancy can be used for more than just controlling internal forces [7]. Increasing the workspace, removal of singularities, decreasing joint forces, and improving dexterity are all possible with this technique.

This paper is concerned with the design optimization of the said mechanism, which consists of determining fixed geometric parameters in accordance with some set objectives. For any design problem, there will potentially be many objectives that cannot all be satisfied simultaneously. In addition, technological constraints must be considered before a practical design can be realized. Here, the focus is on kinematics and on the determination of a *range* of good designs from this perspective.

Purely numerical methods of optimization are avoided as they would give no insight into the workings of the mechanism. Instead, the approach is to form a hierarchy of objectives. Each objective will be examined in turn to reveal the best designs. The idea is to maximize the high-order objectives such that the low-order objectives satisfy some minimum criteria.

II. Description of the Mechanism

The general case of a spherical fully parallel platform mechanism with linear actuation consists of a movable body attached to n legs with one actuator per leg. Each leg has one prismatic joint interposed between two spherical joints. A point of the platform is constrained by a spherical joint permitting freedom of orientation (see Fig. 1). Let us denote the center of rotation as C, the point of attachment of each leg to the platform as P_i, and the point of attachment of each leg to a fixed frame A_i, $i = 1, ..., n$. For the nonredundant case, $n = 3$, with $n > 3$ for all the redundant cases. The parallel mechanism to be described will have four actuators, one being "redundant"—yet essential!

Manuscript received June 8, 1990; revised March 9, 1992. This work was supported by the Natural Sciences and Engineering Research Council of Canada; Les Fonds pour la Formation des Chercheurs et l'Aide à la Recherche, Québec; and the Institute for Robotics and Intelligent Systems Centers of Excellence of Canada.

The authors are with the McGill University Research Center for Intelligent Machines, Montreal, Qc, H3A 2A7, Canada.

IEEE Log Number 9202284.

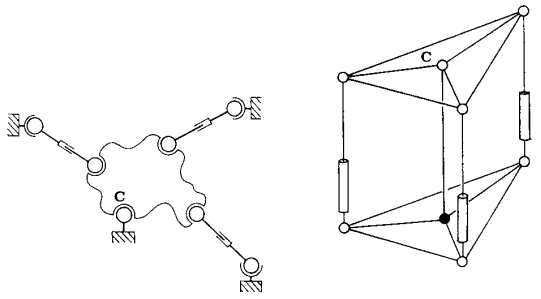

Fig. 1. (a) General case of a fully parallel mechanism. Point C is fixed, preventing translations but permitting arbitrary rotations. The particular case shown in (b) has a debilitating singularity in the middle of the workspace.

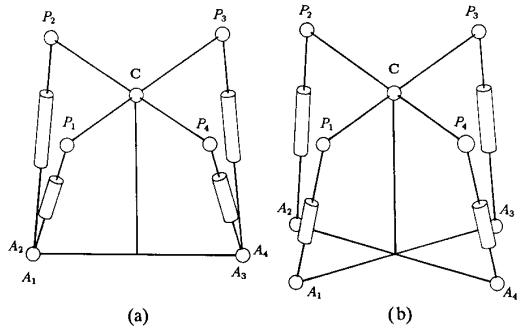

Fig. 2. Schematic arrangement of (a) a separated and (b) a grouped actuator redundant manipulator.

Among all possible ways to configure this mechanism, we will discuss some interesting cases that will arise from the attempt to introduce simplifying symmetries. It is first assumed that C should be in the plane formed by P_i. In the absence of particular constraints, it is reasonable to place the attachment points to the mobile platform (P_i) in a symmetrical arrangement. Under these conditions, simple geometrical descriptions can be adopted. The primary goal of this design is to maximize the usable workspace, as a small workspace is a deficiency of most parallel mechanisms. The workspace limit is reached either when an actuator touches one of the trusses or when two actuators intersect. Interestingly, in all practical implementations we could think of, the orientation workspace always is limited by self-interference and never because of a kinematic singularity condition [7]. By grouping the fixed attachment points in pairs so that $A_1 = A_2$ and $A_3 = A_4$, we eliminate a source of self-collisions of the grouped actuators and enlarge the workspace. This leads to the basic concept of a mechanism depicted in Fig. 2. The nomenclature, as well as the coordinate frames and variables to be used as part of the design optimization are now defined.

The rotation matrix ${}^{B}\boldsymbol{Q}$ with respect to base coordinates centered in C is described by three Euler angles ψ, ϕ, and θ, where ψ is a rotation about the x axis, ϕ is a rotation about the new y axis, and θ is a rotation about the new z axis: ${}^{B}\boldsymbol{Q} = \mathrm{Rot}_x(\psi)\mathrm{Rot}_y(\phi)\mathrm{Rot}_z(\theta)$.

Euler angles suffer from many problems: they are are not unique nor invariant, the geometry of orientations in these coordinates are contorted, they suffer from degenerate points, they are cumbersome to manipulate mathematically, and they are computationally expensive. However, they have the relative benefit of being easy to visualize when compared with other representations. Because of this, the results of this paper are presented in terms of the above set of Euler angles, considering that any simple implementation would be unable to tilt by more than 90°. In this restricted domain, the magnitudes of the tilt angles ψ and ϕ will be less than 90°. The angle θ represents the swivel of the mechanism about the outward pointing normal of the platform, without such restriction.

The solutions to the forward and inverse kinematics problems have been presented in [7]. Is is fortunate that a closed-form solution to the forward problem exists as it is often quite a difficult problem for parallel mechanisms. By performing a velocity analysis we can solve for the Jacobian. The defining equation of the Jacobian $\boldsymbol{J}$ is $\dot{\boldsymbol{\rho}} = \boldsymbol{J}\omega$, where $\dot{\boldsymbol{\rho}}$ is the 4×1 vector of actuator rates, and ω is the 3×1 vector of angular velocity. As expected, the inverse Jacobian is much easier to solve for than the forward one, as the actuator velocities can be readily obtained as linear combinations of the angular velocity. The 4×3 Jacobian matrix $\boldsymbol{J}$ is explicitly known, and from it the loci of singularities of the four submechanisms were derived [7].

A remarkable feature resulting from the addition of a fourth redundant actuator is the "elimination" of the loci of singularities. It is in fact possible to show that, for the grouped actuator case, all singularities are eliminated except when the plane containing points P_i also contains A_i's ($\phi = \pm 90°$). The equivalent mechanism with only three actuators has several debilitating singularities within the usable workspace. This illustrates one use for actuator redundancy, namely, the elimination of singularities. Other significant benefits imparted by actuator redundancy are the ability to control internal forces in the mechanism, and improvement of the accuracy and dexterity.

Assuming perfect spherical joints, the workspace of this mechanism has also been investigated. It was found that the one important factor is the combined thickness of the actuators and central post (t) in relation to the base offset length l_b, defined as the half distance between opposite A points. The singularities are in fact outside the workspace for any realistic design. Fig. 3 plots the range of swivel angle θ versus the tilt angles ϕ and ψ for $l_b/t = 20, 10, 5$. The plots are reasonably flat showing a large usable workspace with over 230° of swivel throughout. The uniformity and volume of the workspace increases as l_b/t increases. In the limiting case, if the actuators have zero thickness, then the boundary of the workspace would occur when $-90° < \psi, \phi < 90°$ and $-135° < \theta < 135°$ irrespective of any other design parameter. In addition, we have found gimbal arrangements for the implementation of each of the spherical joints that do not lead to any kinematic "lock" throughout the interference-free workspace.

We have just summarized the properties of a *combinatorial* mechanism, which shares the overall properties of any parallel mechanisms while overcoming a significant disadvantage. The rest of this paper describes the efforts that were made to take full advantage of these properties from a kinematic point of view.

III. Optimization of the Parallel Mechanism

A. Formulation of the Optimization Problem

The methodology used here to optimize the mechanism can be broken down into two stages. The first stage consists of simplifying the problem by reducing the number of independent variables down to a manageable set. The points of attachement of the four actuators, A_i and P_i, yield 24 variables. Numerical optimization on this set would be quite cumbersome. A symmetrical layout of points P_i reduces the number of independent variables to 13. In order to maximize the workspace by limiting the collisions of actuators, points A_i are grouped, giving the three design variables l_p, l_b, and l_d. The variable l_p is the length of the center post giving the height of the mechanism. The base offset length l_b specifies the width of the mechanism, and l_d is the lever length specifying the dimension of the mobile

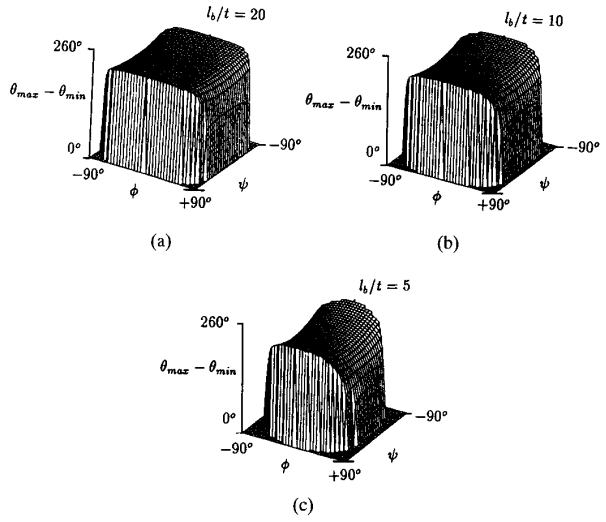

Fig. 3. Workspace of the grouped actuator manipulator. Actuators and trusses are composed of cylinders with an aspect ratio of (a) 20, (b) 10, and (c) 5. The range of possible θ is plotted for each value of ϕ and ψ. Notice that, for practical considerations, the workspace is independent of ϕ and ψ except when they assume large values.

platform. Notice that all three variables have the dimension of length. In terms of kinematics, the scale of the mechanism will have no effect. Arbitrarily, l_d will be set equal to one, and l_b and l_p will be the two independent design variables. Now that we have simplified the problem from 24 to 2 variables, a numerical method will be used to optimize the design according to some objective function.

For the second stage, the mechanism is numerically optimized according to a primary objective function expressing the desired performance. Secondary objectives will then be investigated to ensure that any resulting designs satisfy certain minimum criteria. Even though this methodology may not give precise or unique solutions, an understanding of the mechanism is developed. A strictly numerical approach would not lend any insight into the problem.

B. Selection of the Objective Function

1) Primary Objective—Dexterity: One important consideration in the design of all robotic manipulators is their dexterity. Intuitively we have some idea of dexterity, such as the ease and accuracy with which objects can be manipulated. There have been several attempts to quantify this, each with their own advantages and disadvantages.

The focus has been placed on kinematics rather than dynamics, and therefore a measure of dexterity in terms of the Jacobian will be used. Klein and Blaho [11] compared several of these measures and found that the condition number of the Jacobian matrix was the preferred index because it has a direct physical significance as seen in the following relations given by Salisbury and Craig [14]:

$$\frac{\|\delta\omega\|}{\|\omega\|} \leq k(\boldsymbol{J})\frac{\|\delta\dot{\boldsymbol{\rho}}\|}{\|\dot{\boldsymbol{\rho}}\|} \tag{1}$$

$$\frac{\|\delta\boldsymbol{f}\|}{\|\boldsymbol{f}\|} \leq k(\boldsymbol{J})\frac{\|\delta\boldsymbol{n}\|}{\|\boldsymbol{n}\|} \tag{2}$$

where $\boldsymbol{n}$ is the external moment applied to the mechanism, $\boldsymbol{f}$ is the 4×1 vector of joint forces, and $k(\boldsymbol{J})$ is the condition number of the Jacobian matrix. The condition number is a local measure dependent solely on the configuration. From (2) we see that the condition number gives the amplification factor of relative errors when going from joint to Cartesian coordinates. It can also be thought of as a measure of sensitivity to external perturbations. If $\delta\boldsymbol{n}$ is a small disturbance, then the condition number gives an upper bound on the resulting relative change in joint forces. The knowledge of the condition number is thus a primary factor in the selection of sensors and actuators to achieve a given performance. Conversely, bounds on the performance of the mechanism can be derived from the properties of given sensors and actuators. As a measure of dexterity, the condition number is related to the accuracy of the mechanism in a specific configuration. The condition number ranges in value from one (isotropy) to infinity (singularity) and thus can be regarded as a measure of the "distance" the particular configuration is from a singularity [1].

Given task specifications, other indices such as the actuation index [9] and the compatibility index [4] could be used. For cases in which the dynamics of the manipulator is important, uniformity of the inertia matrix [2] or dynamic manipulability [18] could be important considerations. The optimization is being carried out independently of a specific task for greater generality, and so these measures would not be appropriate.

Any $m \times n$ matrix $\boldsymbol{J}$ can be factored into the following form, known as the singular value decomposition:

$$[\boldsymbol{J}]_{m\times n} = [\boldsymbol{U}^T]_{m\times m}[\boldsymbol{\Sigma}]_{m\times n}[\boldsymbol{V}]_{n\times n} \tag{3}$$

where $\boldsymbol{U}$ and $\boldsymbol{V}$ are orthogonal matrices and $\boldsymbol{\Sigma}$ is a diagonal formed with the singular values. For $m = 4$ and $n = 3$, we have the three singular values $\sigma_1 \geq \sigma_2 \geq \sigma_3 \geq 0$. The condition number can be expressed in terms of these singular values: $k(\boldsymbol{J}) = \sigma_1/\sigma_3$. The reciprocal of the condition number will be used as the measure of local dexterity: $D_l = 1/k(\boldsymbol{J})$ ranges from 0 (singularity) to 1 (isotropy). For purposes of design we need a global dexterity index independent of the orientation of the platform. The integral of the local dexterity measure over the workspace, as defined in [3], could be one such possibility. Another is the global conditioning index as in [6], given by

$$D_g = \frac{\int_{\mathcal{W}} D_l dw}{\int_{\mathcal{W}} dw} = \frac{\int_{\mathcal{W}} 1/k(\boldsymbol{J}) dw}{\int_{\mathcal{W}} dw}. \tag{4}$$

This is the dexterity integrated over the workspace and normalized by the volume of the workspace. It gives a measure in the range $0 \leq D_g \leq 1$ that is independent of the size of the workspace, unlike a simple integral. For this reason, D_g will be used as the objective function to be maximized over the design variables.

One of the problems with an integral measure is that it represents an average and therefore does not take into account any poor local behavior exhibited by the manipulator. Two additional indices will be presented as secondary objectives. These will be selected to help pinpoint a good design as well as to provide the designer with a better insight into the workings of the mechanism.

2) Secondary Objective—Actuator Forces: The first index is once again related to the singular values of the Jacobian. For a parallel mechanism, the Jacobian maps the joint forces $\boldsymbol{f}$ to the external moment $\boldsymbol{n}$ under the condition of static equilibrium as follows:

$$\boldsymbol{n} = \boldsymbol{J}^T\boldsymbol{f}. \tag{5}$$

Using the left pseudoinverse, the minimum norm solution to this equation is

$$\boldsymbol{f} = \boldsymbol{J}(\boldsymbol{J}^T\boldsymbol{J})^{-1}\boldsymbol{n}. \tag{6}$$

From the singular value decomposition theorem we can place bounds on $\|\boldsymbol{f}\|$

$$\|\boldsymbol{n}\|/\sigma_1 \leq \|\boldsymbol{f}\| \leq \|\boldsymbol{n}\|/\sigma_3. \tag{7}$$

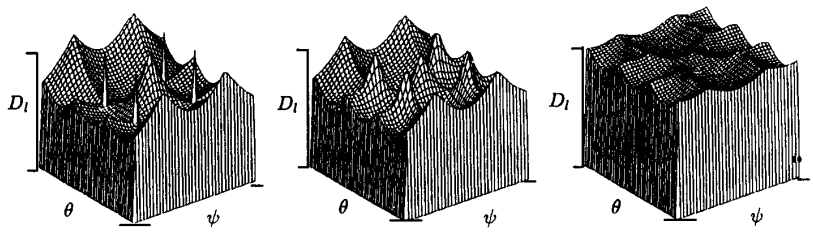

(a) (b) (c)

Fig. 4. Local dexterity D_l of the mechanism for three isotropic designs plotted on a scale that varies from 0 to 1. For each plot the angle θ varies in a range $\pm 135°$ and ψ in a range $\pm 90°$. When (a) $l_b = l_p = 0.7$, several of the isotropic points are "spikes" that would not serve as good operating points. For $l_b = l_p$ equal to (b) 1 and (c) 5, the flatness of these points increases resulting in superior designs.

For parallel manipulators, one of the characterizing features of the region surrounding a singularity is the abnormally low joint velocities. In terms of statics, the joint forces should approach infinity as one nears a singularity. For a given external moment, the minimum singular value provides an upper bound on the magnitude of joint forces. Maximizing this value would reduce the force along the actuators and hence keep the mechanism well conditioned. Thus, we define $F_l = 1/\sigma_3$ as a secondary local measure for purposes of optimization. There is no maximum value for F_l, but there is a minimum of zero when the mechanism is singular. Once again we integrate this measure over the workspace to form a global measure F_g that can be used for design.

$$F_g = \frac{\int_{\mathcal{W}} F_l dw}{\int_{\mathcal{W}} dw} = \frac{\int_{\mathcal{W}} 1/\sigma_3 dw}{\int_{\mathcal{W}} dw}. \tag{8}$$

3) Another Secondary Objective—Uniformity: Maximizing the global indices D_g and F_g is not enough to ensure a good design, as this gives no indication of the uniformity of the dexterity over the workspace. The relative variation of these measures should be kept as small as possible to make the dextrous regions more consistent and useful. Portions of tasks requiring high accuracy can then be structured about operating points of maximum dexterity. These configurations would be of little use if the dexterity in the immediate neighborhood dropped drastically. Any small rotation would then reduce the dexterity resulting in a configuration with a high sensitivity to errors, an amplification of noise, and poor controllability. Consider the three plots of dexterity in Fig. 4, all of isotropic designs with $l_p = l_b$. As l_b approaches $1/\sqrt{2}$, the dexterity in the vicinity of the isotropic points degrades and becomes more spiky. Notice that $\psi = \pm 45°$, $\theta = \pm 45°$, $\phi = 0$, and $l_b = l_p = 1/\sqrt{2}$ causes one of the actuator lengths ρ to go to zero and the determinant of the Jacobian to become unbounded, and hence singular.

One way to check the uniformity of any function is to look at the magnitude of its gradient. Thus, a local measure of flatness of the dexterity would be $GD_l = \|\nabla D_l\|$. Integrating this to obtain a global measure would obviously not be a good idea. Thus, we define the global gradient index as

$$GD_g = \max_{\mathcal{W}} GD_l = \max_{\mathcal{W}} \|\nabla D_l\|. \tag{9}$$

If GD_g is zero, then the dexterity is uniform throughout the workspace. Taken alone this is not necessarily good, as the dexterity could be uniformly bad, everywhere. As GD_g increases, the dexterity will become less uniform and spikier in at least one point in the workspace.

IV. Carrying Out the Optimization

A. Computational Issues

The objective function used to optimize the design is based on an integral of the dexterity defined in terms of the singular values of the Jacobian. This function does not have an analytic form. The singular values can be computed numerically with good accuracy, but this requires a large amount of computational time. The integral of the dexterity must also be computed numerically as no closed-form solution exists. Since function evaluations are expensive, the integral will be approximated by a discrete sum.

$$\int_{\mathcal{W}} D_l dw \approx \sum_{w \in \mathcal{W}} D_l \tag{10}$$

where w is one of N_w points in the workspace of the mechanism. Therefore

$$D_g \approx \frac{1}{N_w} \sum_{w \in \mathcal{W}} D_l. \tag{11}$$

For the sum to approximate the integral, the orientations w should be uniformly distributed across the workspace. A uniform sampling of the three Euler angles will obviously not be appropriate. Finite rotations can be conveniently interpolated using quaternion coordinates, four-dimensional quantities composed of a scalar part q_0 and a three-dimensional vector part $\vec{v}$, $\boldsymbol{q} = (q_0, \vec{v})$, where $\vec{v} = (q_1, q_2, q_3)$. In terms of Euler's theorem, any rotation of a rigid body can be expressed as a rotation about an axis $\hat{\boldsymbol{u}}$ by an angle θ. This is related to quaternions as follows: $q_0 = \cos(\theta/2)$ and $\vec{v} = \hat{\boldsymbol{u}} \sin(\theta/2)$. Thus, any rotation can be represented by a quaternion of unit magnitude, $\|\boldsymbol{q}\| = 1$. Since a rotation of $\theta + 2\pi$ about $\hat{\boldsymbol{u}}$ is identical to a rotation of θ about $\hat{\boldsymbol{u}}$, it can be shown that $\boldsymbol{q}$ and $-\boldsymbol{q}$ are in fact the same rotation. Thus, the space of rotations falls on the upper half hypersphere $\|\boldsymbol{q}\| = 1$.

The problem can now be stated as how to uniformly sample the unit hypersphere. In general, no closed-form solution exists for this problem. In 3D only the vertices of the regular polyhedra with triangular faces lead to a uniform sampling. The largest is the icosahedron each with 12 vertices. For more points we can subdivide the faces of these solids and project the resulting vertices onto the unit sphere. Although this does not give an exact uniform distribution, it is nonetheless a good approximation. This technique, popularized by R. Buckminster Fuller, has been used extensively to construct geodesic domes from a subdivided icosahedron. For an even better distribution of points, we can combine the vertices of the icosahedron with its dual, the dodecahedron, and then subdivide the faces.

As in the 3D case, the vertices of the regular polytopes are used, and if more are needed, then the faces are subdivided and

projected onto the unit hypersphere. The regular polytopes have been enumerated [5]. The largest has 600 vertices. For more vertices, we can subdivide the 120 tetrahedral cells of its dual and project the resulting points onto the unit hypersphere, resulting in 720 points on the unit hypersphere, each separated by approximately the same distance. Only the set of rotations that lie inside the workspace of the manipulator are used when forming the global dexterity measure, reducing the number of rotations from 720 to 368. This is enough to use in (11) to approximate the integral by a discrete sum. From symmetry considerations the dexterity need only be evaluated in one quadrant of the workspace, and so the number of points effectively reduces to 92. Since each evaluation of the local dexterity is expensive, we would not want to use more than this number of points.

Since we have no closed-form representation of the local dexterity, the gradient measure GD_l must be approximated numerically. Once again the computational complexity of the singular value decomposition is a limiting factor, and so the gradient will be approximated by first-order difference equations. Quaternions are the natural choice of coordinates for doing interpolations of rotations, and hence the gradient operation will be performed in this coordinate system. One problem with this method is that only three elements of the quaternion are independent. Thus, the gradient can be approximated by only three first-order difference equations as follows:

$$\nabla D_l = \left[\frac{\partial D_l}{\partial q_1}, \frac{\partial D_l}{\partial q_3}, \frac{\partial D_l}{\partial q_3}\right] \tag{12}$$

where

$$\frac{\partial D_l}{\partial q_1} \simeq \frac{D_l(q_1 + \Delta q_1, q_2, q_3) - D_l(q_1, q_2, q_3)}{\Delta q_1}. \tag{13}$$

The remaining partials are found similarly. The global flatness measure GD_g is approximated by calculating the maximum of GD_l over the 92 points defined above. This requires four evaluations of D_l for each orientation for a total of 368 evaluations for each set of design variables.

Although the optimization will take place on the above global measures, it is still important to examine the local behavior of the mechanism in terms of dexterity.

B. Local Behavior of the Mechanism

Ideally, we would like the mechanism to be as accurate as possible throughout the workspace. It is impossible for the mechanism to be isotropic everywhere; however, for many applications involving delicate work it is sufficient for the manipulator to be isotropic in a discrete set of orientations. These optimal configurations could then serve as an operating point for much of the task. Placing one of these configurations at the center of the workspace would yield the maximum benefit.

The Jacobian is isotropic only if it is proportional to an orthogonal matrix. This implies that the columns are mutually orthogonal and that they all have the same magnitude. The Jacobian at the center of the workspace (Euler angles $\psi = \phi = \theta = 0$) is given by

$$\boldsymbol{J} = \frac{1}{\sqrt{1/2 + (1/\sqrt{2} - l_b)^2 + l_p^2)}} \begin{bmatrix} l_p & l_p & -l_b \\ l_p & -l_p & l_b \\ -l_p & -l_p & -l_b \\ -l_p & l_p & l_b \end{bmatrix}. \tag{14}$$

Only when $l_b = l_p$ is the Jacobian isotropic in this configuration.

Fig. 5 plots the dexterity of the manipulator over the workspace when $l_b = l_p = l_d = 1$. It is interesting to note that there are several configurations where the mechanism is isotropic (see Table I). These configurations also correspond to maxima of the dexterity

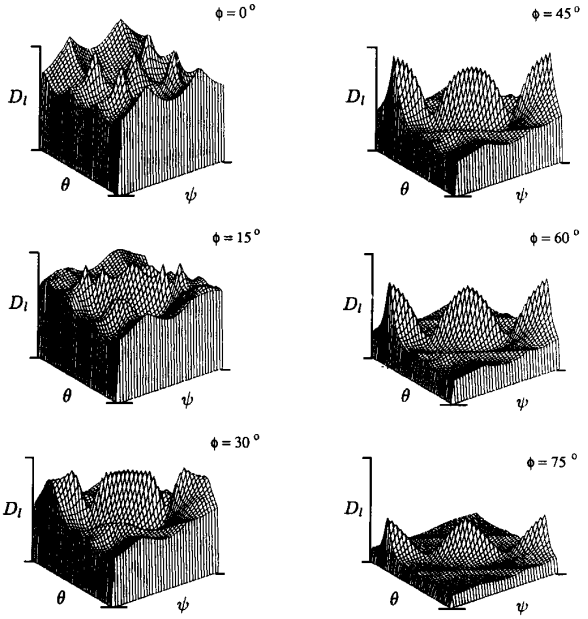

Fig. 5. Dexterity D_l of the grouped actuator parallel mechanism plotted on a scale that varies from 0 to 1. Here, $l_d = l_p = l_b = 1$. The three-dimensional plots are of the local dexterity D_l versus two Euler angles ψ varying in the range $\pm 90°$ and θ in the range $\pm 135°$. Each plot is done for a different value of ϕ. Notice the isotropic points ($D_l = 1$) present for $\phi = 0$ and $\phi = 45°$. When $\phi = 90°$ the manipulator is in a singular configuration, thus the dexterity is identically zero.

TABLE I
ISOTROPIC CONFIGURATIONS FOR $l_b = l_d = l_p = 1$ RANKED BY MINIMUM SINGULAR VALUE

ψ	ϕ	θ	Minimum Singular Values
0	0	0	1.12
90	±45	90	1.00
–90	±45	–90	1.00
±45	0	±45	0.82
±45	0	±135	0.82

gradient. As the tilt angle ϕ increases, there is an overall loss of dexterity culminating in the singularity ($D_l = 0$) when $\phi = \pm 90°$. Roughly speaking, the dexterity is high anywhere in the range $|\phi| \leq 60°, |\psi| \leq 90°, |\theta| \leq 135°$. This provides a large usable workspace free of singularities and well suited for accurate motions.

C. Results of the Optimization

The resulting surface $D_g(l_b, l_p)$ is shown in Fig. 6, where l_b and l_p range in value from 0.1 to 10. The surface is saddle shaped, with no apparent maximum. The ridge of the saddle corresponds to the isotropic designs ($l_b = l_p$) forming a locus of highest dexterity (Fig. 7). The maximum values of D_g occur when $(l_b, l_p) \to (\infty, \infty)$ and $(l_b, l_p) = (\epsilon, \epsilon)$ where $\epsilon \to 0$. The first maximum *does not lead* to a realistic design, as the link lengths tend to infinity. The second design is equally bad because $l_p = l_b = 0$ causes the singular values of the Jacobian to be uniformly zero and hence the manipulator is singular. Only in the limit is the dexterity high. This can be clarified by looking at the secondary objective function F_g, which takes the average of the minimum singular value over the workspace.

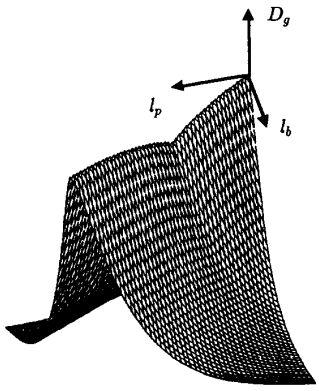

Fig. 6. The global dexterity D_g as a function of l_b and l_p. These lengths range in value from 0.1 to 10 on a logarithmic scale. There is no optimal value for this "saddle" shaped function. The highest dexterity occurs along the ridge $l_b = l_p$, the isotropic designs.

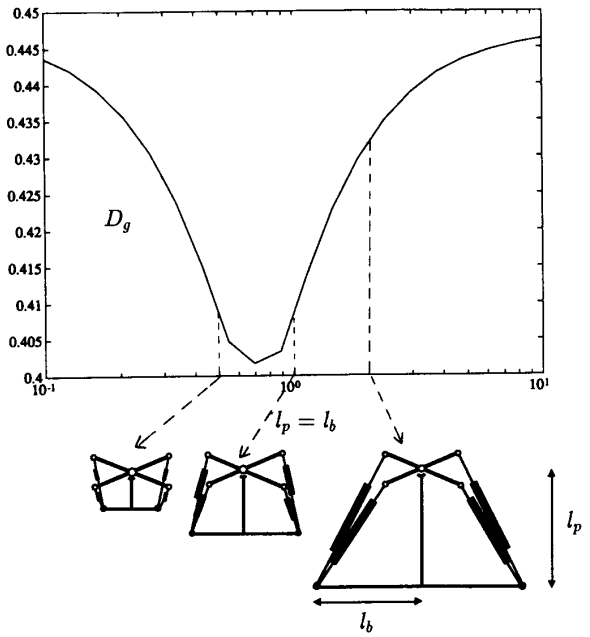

Fig. 7. The global dexterity of the isotropic designs for various values of $l_b = l_p$ when $l_d = 1$. Shown are also some isotropic designs and their corresponding location on the curve.

Since the condition number was incapable of finding an optimal design, we will try to maximize one of the secondary objectives, namely, to have the largest average minimum singular value (F_g). This function is plotted for various designs in Fig. 8. Once again the best designs in this respect are those that attain isotropy. Unlike the previous optimization, only those designs with large values for l_b and l_p give good results, while those with small values of the design variables cause F_g to decrease toward zero. Next, a numerical maximization of F_g was performed using Powell's multidimensional method [16]. A single maximum was found for $l_b = l_p = 36$, but it does not lead to a reasonable design either! The maximum is in fact quite broad with the function showing little difference when the design lengths change by a factor of 100.

The uniformity of the dexterity measures should now be checked to ensure that the final design will have a consistent and predictable behavior. Fig. 9 shows the maximum gradient of the dexterity (GD_g) over the design variables. The magnitude of the gradient approaches infinity for $l_b = l_p = 1/\sqrt{2}$ when one of the actuator lengths can go to zero. It is interesting to note that the global dexterity for this design *is not low*, even though it contains a singularity of the Jacobian. The ability to detect this condition is one of the justifications for using the gradient method. The flatness of the dexterity is maximized when l_b approaches infinity or zero, and is quite good everywhere except in the vicinity of $1/\sqrt{2}$.

Although maximization of the global dexterity was unable to produce a realizable design, it is possible to describe a space that yields interesting designs. This is done by specifying some minimum criteria for the performance indicators. One such rule could be to permit designs for which the performance is within a certain percentile of the maximum (see Fig. 10).

Last, physical realizability will impose additional constraints on the design variables. An acceptable heuristic would be to select a design within the region of interest such that the lengths l_p and l_b are as small as possible resulting in a compact device. Another possibility would be to consider only those designs that are isotropic within the region of interest to improve the local dexterity. Combining these two heuristics leads to the selection of an isotropic mechanism with minimum design lengths. This rule results in $l_b = l_p = 2$ for D_g and F_g specified at 95% of the maximum. A summary of the optimization procedure is outlined as follows:

1) Define heuristics
   a) Improve local dexterity → isotropic designs ($l_b = l_p$).
   b) Reduce the length l_b and l_p to keep the mechanism compact.
2) Set minimum performance standards for the global dexterity, maximum actuator forces, and uniformity of the dexterity (D_g, F_g, and GD_g respectively).
3) Search the resulting region for the best design according to the above heuristics.
4) Test if this solution is feasible. Does it comply with other design constraints (mechanical, application specific, . . .)? If not, return to step 2.

V. Summary and Conclusion

The architecture of actuator redundant mechanism has been established and then optimized from a kinematic view point. This consists of determining fixed geometric parameters in accordance with some set objective. The general form of this simple mechanism can be described by over 20 parameters. Any brute force attempt at numerical optimization would be computationally intractable. Even if this were possible, it would give no insight into the workings of the mechanism.

The approach taken here is to form a hierarchy of objectives. Each objective is examined in turn to reveal the best designs. The idea is to maximize the high-order objectives such that the low-order objectives satisfy some minimum criteria. For parallel mechanisms the overriding concern is to provide a large and uniform workspace. Maximization of the workspace volume is used to restrict the possible designs thereby reducing the number of design parameters to a manageable set. Interestingly, maximizing the dexterity and minimizing the maximum actuator forces, although possible in principle, do not lead to physically realizable designs, despite their relevance for sensing and actuation. This shows the care that must exercised in ascribing utility to simple measures. Among many alternatives, the

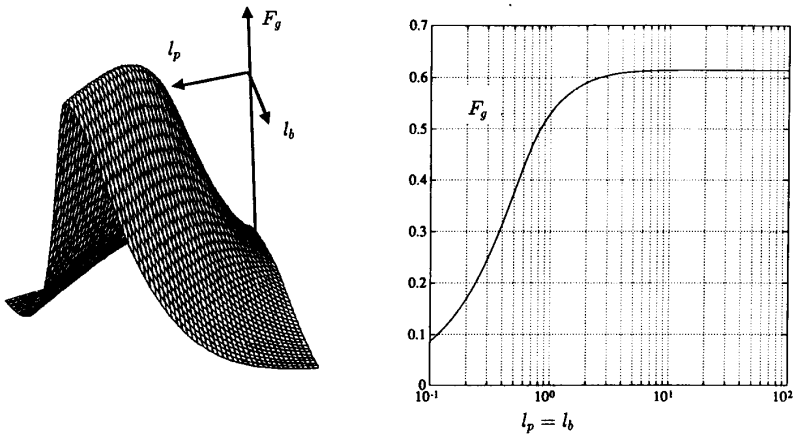

(a) (b)

Fig. 8. F_g as a function of l_b and l_p. The average minimum singular value is high when the two design lengths are equal and above 1. Also shown is F_g versus the isotropic designs ($l_b = l_p$). The maximum is quite broad with no sharp peak.

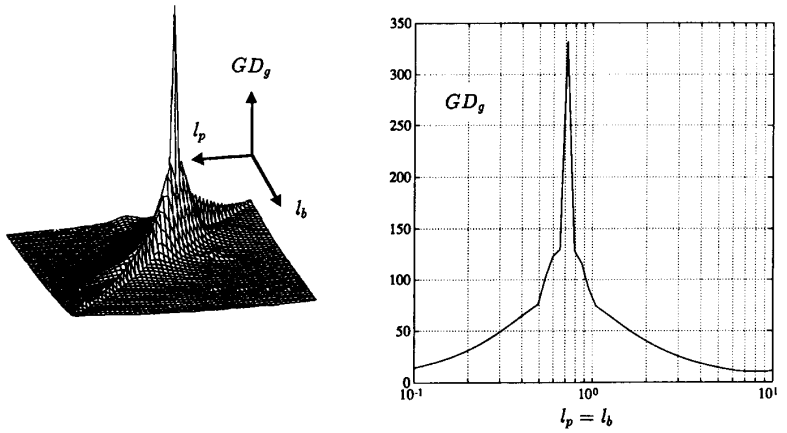

(a) (b)

Fig. 9. The maximum gradient norm of the dexterity GD_g versus the design variables. The further one is from the point $l_b = l_p = 0.707$, the better behaved the dexterity. In (a), l_b and l_p range from 0.1 to 10. The isotropic designs are shown in (b) where $l_b = l_p$.

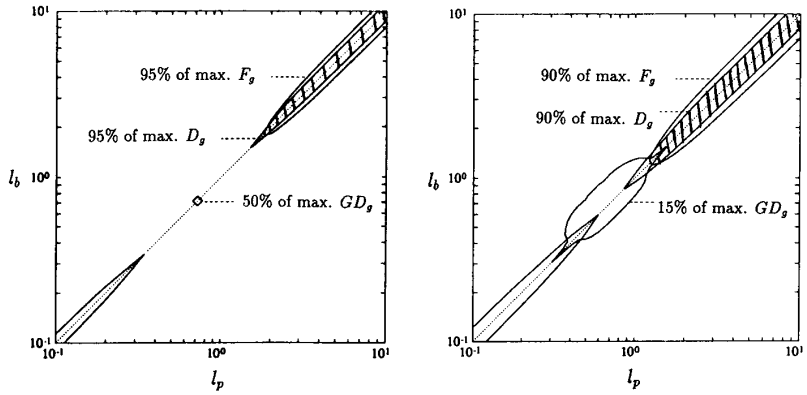

Fig. 10. Regions of interesting designs are obtained from the intersections of areas of high performance. This results from thresholding the measures D_g, F_g, and GD_g at certain percentiles of the maximum. The regions of interest are shaded. The dotted line corresponds to those designs that are isotropic at some point in the workspace.

smoothness of the dexterity can be used effectively as additional possible secondary objectives.

The methodology outlined in this paper is intended to be a general guideline for the optimization of robotic mechanisms. For the specific case of this parallel mechanism, a range of designs was found to be good in terms of dexterity, but this should be only one consideration among many in the design process. Evidently, no system exists to unambiguously define these heuristics; however, this methodology does provide an informative framework in which the mechanism can be analyzed.

At the time of this writing, a hydraulically actuated version of the described mechanism is under construction. It is intended to form the shoulder of a high-performance manipulator, and its parameters have been determined following the guidelines outlined in this paper. Many other applications of the described mechanism are possible resulting in various designs.

ACKNOWLEDGMENT

The authors wish to acknowledge the anonymous referees for their comments. V. Hayward would also like to thank Prof. K. H. Hunt, Prof. J. Phillips, and Prof. S. C. Jacobsen, as well as the late Dr. M. McKinnon for their encouragement.

REFERENCES

[1] J. Angeles, "Isotropy criteria in the kinematic design and control of redundant manipulators," in *Robots with Redundancy: Design, Sensing and Control, (NATO Series*, A. Bejczy, Ed. New York: Springer.

[2] H. Asada, "A geometrical representation of manipulator dynamics and its application to arm design." *ASME J. Dynam. Syst. Meas., Contr.*, vol. 105, no. 3, pp. 131–135, 1983.

[3] H. Asada and J. A. Cro Granito, "Kinematic and static characterization of wrist joints and their optimal design," in *Proc. IEEE Int. Conf. Robotics Automat.* (St. Louis, MO), 1985, pp. 244–250.

[4] S. L. Chiu, "Task compatibility of manipulator postures," *Int. J. Robotics Res.*, vol. 7, no. 5, pp. 13–21, 1988.

[5] H. S. M. Coxeter, *Regular Polytopes*. New York: MacMillan, 1963.

[6] C. Gosselin, "Kinematic analysis, optimization and programming of parallel robotic manipulators," Ph.D. dissertation, Dept. of Mechanical Eng., McGill Univ., Montreal, Canada, 1988.

[7] V. Hayward and R. Kurtz, "Modeling of a parallel wrist mechanism with actuator redundancy," in *Advances in Robot Kinematics*, S. Stifter and J. Lenarčič, Eds. New York: Springer, 1991.

[8] V. Hayward, "Borrowing some design ideas from biological manipulators to design an artificial one," in *Robots and Biological Systems, NATO Series*, P. Dario, P. Aebisher, and G. Sandini, Eds. New York: Springer, 1991.

[9] S. Hirose and M. Sato, "Coupled drive of the multi-DOF robot," in *Proc. IEEE Int. Conf. Robotics Automat.*, 1989, pp. 1610–1616.

[10] K. H. Hunt, "Structural kinematics of in-parallel-actuated robot arms," *ASME, J. Mech., Transmission, Automat. Design.*, vol. 105, pp. 705–712, 1983.

[11] C. A. Klein and B. E. Blaho, "Dexterity measures for the design and control of kinematically redundant manipulators," *Int. J. Robotics Res.*, vol. 6, no. 2, pp. 72–83, 1987.

[12] J. Lenarčič, A. Umek, and S. Savic, "Considerations on human arm workspace and manipulability," in *Advances in Robot Kinematics*, S. Stifter and J. Lenarčič, Eds. New York: Springer, 1991.

[13] J. P. Merlet, "Force feedback control of parallel manipulators," in *Proc. IEEE Int. Conf. Robotics Automat.* (Philadephia, PA), 1988, pp. 1484–1489.

[14] J. K. Salisbury and J. Craig, "Articulated hands: Force control and kinematic issues," *Int. J. Robotics Res.*, vol. 1, no. 1, pp. 4–17, 1982.

[15] M. Sklar and D. Tesar, "Dynamic analysis of hybrid serial manipulator systems containing parallel modules," *ASME J. Dynam. Syst. Meas. Contr.*, vol. 110, pp. 109–115, 1988.

[16] W. H. Press, B. P. Flannery, S. A. Teukolsky, and W. T. Vetterling, *Numerical Recipes in C: The Art of Scientific Computing*. Cambridge, U.K.: Cambridge Univ. Press, 1988.

[17] K. J. Waldron and K. H. Hunt, "Series-parallel dualities in actively coordinated mechanisms," *Int. J. Robotics Res.*, vol. 10, no. 5, pp. 473–480, 1991.

[18] T. Yoshikawa, "Analysis and design or articulated robot arms from the viewpoint of dynamic manipulabity" in *Proc. Robotics Res.: 3rd Int. Symp.*, O. D. Faugeras and G. Giralt, Eds. Cambridge, MA: MIT Press, 1986, pp. 273–279.

An Approach to Discrete Inverse Dynamics Control of Flexible-Joint Robots

Krzysztof P. Jankowski and Hendrik Van Brussel

***Abstract*—This paper presents an inverse-dynamics-based method for discrete-time control of flexible-joint robots. The main drawbacks of the inverse dynamics approach based on continuous-time analysis are its computational burden and the necessity for very high sampling frequencies. These inconveniences can be avoided by the use of numerical methods conceived for the solution of systems of differential-algebraic equations. Such an approach naturally leads to a predictive control scheme. As a consequence, in the control process a basic dynamic model of a flexible-joint robot can be used, which is much less complex than in the classical inverse dynamics solution. At the same time, the simplified inverse dynamics approach discussed here accepts low sampling frequencies. Control algorithms are presented and their properties are discussed. Successful experiments on computer control of a two-link manipulator with one flexible joint are described.**

I. INTRODUCTION

The existence of flexibilities in the robot structure limits its ability to perform high-precision manipulation. Experimental results reveal that, for a wide variety of robots, joint flexibility is the principal source contributing to overall robot flexibility [1]. Therefore, joint flexibility should be taken into account in the modeling and design of robot controllers if high performance is to be achieved.

One approach to control of flexible-joint robots is based on the idea of nonlinear decoupling, which can be achieved by applying the feedback linearization method [2], [3]. For system models in the descriptor form, inverse dynamics control can be used to accomplish the same task [4], [5]. These methods have been criticized for their computational complexity and the necessity of feedback of link accelerations and jerks to provide robustness to parameter uncertainty and external disturbances [2].

Using another approach, based on the concept of an integral manifold [2], [6], one has no need for feedback of accelerations and jerks. However, practical implementation of this method is a complicated task, and the robustness to parameter uncertainty is difficult to achieve. Recently, the use of adaptive control methods for

Manuscript received July 15, 1991; revised January 22, 1992.

K. P. Jankowski was with the Department of Mechanical Engineering, Katholieke Universiteit Leuven, B-3030 Leuven, Belgium. He is now with the Flexible Manufacturing Research and Development Centre, McMaster University, Hamilton, Ontario L8S 4L7, Canada.

H. Van Brussel is with the Department of Mechanical Engineering, Katholieke Universiteit Leuven, B-3030 Leuven, Belgium.

IEEE Log Number 9201549.